Nonlinear Luttinger Liquid Plasmons in Semiconducting Single Walled Carbon Nanotubes

Sheng Wang[1,2], Sihan Zhao[1], Zhiwen Shi[3,4], Fanqi Wu[5], Zhiyuan Zhao[5], Lili Jiang[1], Kenji Watanabe[6], Takashi Taniguchi[6], Alex Zettl[1,2,8], Chongwu Zhou[5,7], Feng Wang[1,2,8]*

[1]Department of Physics, University of California at Berkeley, Berkeley, California 94720, USA.

[2]Materials Sciences Division, Lawrence Berkeley National Laboratory, Berkeley, California 94720, USA.

[3]Key Laboratory of Artificial Structures and Quantum Control (Ministry of Education), School of Physics and Astronomy, Shanghai Jiao Tong University, Shanghai 200240, China

[4]Collaborative Innovation Center of Advanced Microstructures, Nanjing, 210093, China.

[5]Department of Chemical Engineering and Materials Science, University of Southern California, Los Angeles, California 90089, USA

[6]National Institute for Materials Science, 1-1 Namiki, Tsukuba 305-0044, Japan.

[7]Department of Electrical Engineering, University of Southern California, Los Angeles, California 90089, USA

[8]Kavli Energy NanoScience Institute at the University of California, Berkeley and the Lawrence Berkeley National Laboratory, Berkeley, California, 94720, USA.

*To whom correspondence should be addressed.

Email: fengwang76@berkeley.edu

Interacting electrons confined in one dimension (1D) are generally described by the Luttinger liquid formalism, where the low-energy electronic dispersion is assumed to be linear and the resulting plasmonic excitations are non-interacting. Instead, a Luttinger liquid in 1D materials with nonlinear electronic bands is expected to show strong plasmon-plasmon interactions, but an experimental demonstration of this behaviour has been lacking. Here, we combine infrared nano-imaging and electronic transport to investigate the behavior of plasmonic excitations in semiconducting single-walled carbon nanotubes with carrier density controlled by electrostatic gating. We show that both the propagation velocity and the dynamic damping of plasmons can be tuned continuously, which is well captured by the nonlinear Luttinger liquid theory. These results are in contrast to the gate-independent plasmons observed in metallic nanotubes, as expected for a linear Luttinger liquid. Our findings provide experimental demonstration of 1D electron dynamics beyond the conventional linear Luttinger liquid paradigm and are important for understanding excited state properties in 1D.

Electrons in three- and two-dimensional metals are well represented by weakly interacting quasi-particles within Fermi liquid theory. However, this theory breaks down in one dimension (1D) where Coulomb interactions become dominant and can qualitatively alter the electronic behaviors. Luttinger liquid theory, which is based on the linearization of the dispersion relation of the particles constituting the fluid, can successfully describe many exotic phenomena in 1D metals such as spin-charge separation and power-law dependence of spectral functions near the Fermi level[1-14]. However, the electronic band dispersion in real 1D systems is often not strictly linear and the linearization taken in Luttinger liquid theory limits its validity to low-energy electron behaviors. In order to describe high-energy quasi-particle excitations and dynamics, novel theoretical approaches have been employed to replace the linear dispersion with a generic one, which is known as nonlinear Luttinger liquid theory[15-22]. This nonlinear theory predicts many intriguing electron behaviors beyond the linear Luttinger liquid paradigm. For instance, the collective electron excitations (i.e. plasmons) in a linear Luttinger liquid are expected to be extremely long-lived due to the absence of an intrinsic relaxation mechanism. However, in a nonlinear Luttinger liquid, the nonlinearity of the band dispersion can strongly mix different plasmon excitations, resulting in a drastic reduction of plasmon lifetime. Such unusual excited state dynamics of a nonlinear Luttinger liquid have rarely been experimentally explored previously.

Here we probe nonlinear Luttinger liquid physics using gated semiconducting single walled carbon nanotubes (SWNTs) as a model system and compare the behavior to that of a linear Luttinger liquid in metallic SWNTs. We systematically vary the carrier density in metallic and semiconducting nanotubes through electrostatic gating while performing in situ infrared nano-imaging as schematically shown in Fig. 1a. We show that the plasmon wavelength, amplitude and quality factor in semiconducting SWNTs can be continuously tuned due to the nonlinear band dispersion. In particular, our results reveal the unusual relaxation dynamics of plasmon excitations in semiconducting SWNTs as described by nonlinear Luttinger liquid theory, and their behaviors

are in marked contrast to those of linear Luttinger liquid plasmon excitations present in metallic SWNTs.

Metallic and semiconducting SWNTs with diameter ranging from 0.7 to 2.0 nm are directly grown on hexagonal boron nitride (h-BN) flakes exfoliated on SiO_2 (285 nm)/Si substrates by chemical vapor deposition (CVD) (see methods for details). SWNTs on h-BN flakes are ultraclean and very long, and can be readily integrated into field-effect transistor (FET) devices [23]. We probe the plasmons in gated nanotube devices at different carrier densities using infrared scanning near-field optical microscopy (SNOM) as illustrated in Fig. 1a[12, 23-25]. This infrared nano-imaging technique is based on a tapping mode atomic force microscopy (AFM). Infrared (IR) light with wavelength 10.6 μm is focused onto the apex of a gold coated AFM tip. The sharp tip with its large momentum simultaneously enables the excitation of the plasmons and scattering of this plasmon field to the far field. The back scattered signal contains essential information about the plasmons and is captured by a mercury cadmium telluride (MCT) detector. The excited plasmon wave propagates along the nanotubes and gets reflected by the nanotube ends or other scatters. The interference between the tip-launched plasmon field and the reflected plasmon field produces a periodic electric field distribution. We probe this periodic electric field by scanning the tip along the nanotube, which enables the real-space visualization of the plasmons.

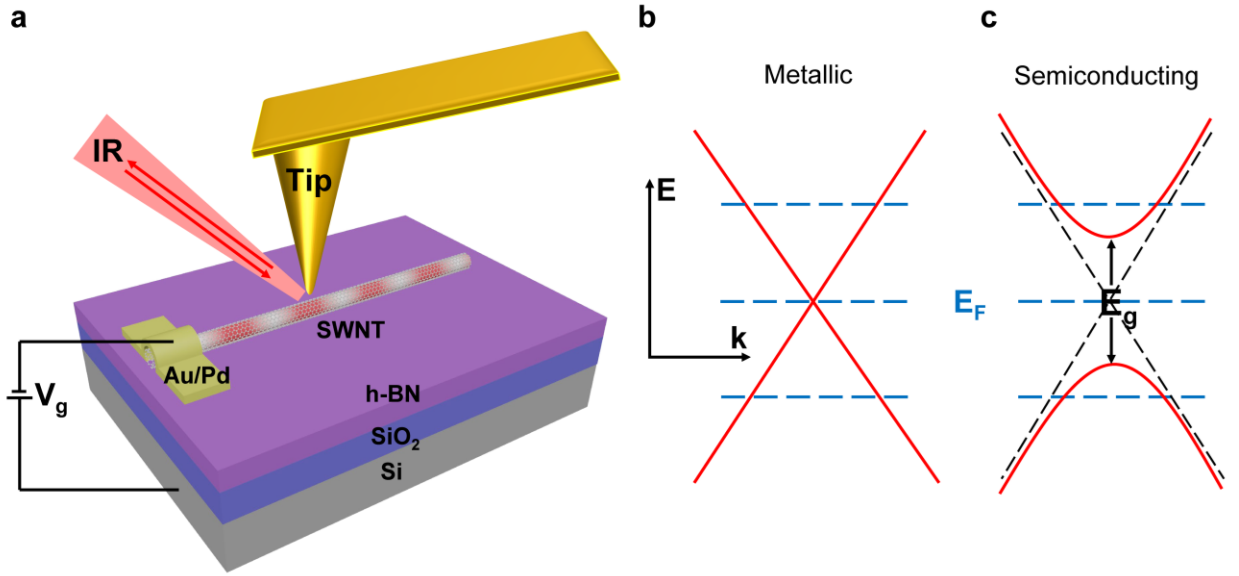

Figure 1| Schematic of SNOM of SWNTs with carrier density controlled by electrostatic gating. a, Schematic of infrared nano-imaging of a nanotube FET device. SWNTs are directly grown on hexagonal boron nitride (h-BN) flakes exfoliated on SiO2 (285 nm)/Si substrates by chemical vapor deposition (CVD). A back gate voltage V_g is applied between the metal electrode (Au/Pd) contacting the SWNT and the Si substrate to tune the carrier concentration in the SWNT. For infrared (IR) nano-imaging, IR light with wavelength 10.6 μm is focused onto the apex of a gold coated AFM tip. The sharp tip with its large momentum enables the excitation of the plasmons. The excited plasmon wave propagates along the nanotubes and gets reflected by the nanotube ends

or other scatters. The interference between the tip-launched plasmon field and the reflected plasmon field produces a periodic electric field distribution schematically illustrated by the interference fringes in the SWNT. Probing of the electric field by scanning the tip along the nanotubes enables the direct visualization of the plasmons. **b**, Band structure of metallic SWNTs. Metallic SWNTs feature a gapless linear energy-momentum (E-k) dispersion schematically shown as the red curve. **c**, Band structure of semiconducting SWNTs. Semiconducting SWNTs feature a hyperbolic E-k dispersion (schematically shown as the red curve) with a finite band gap E_g. The diagonal black dashed lines indicate the linear band structure of metallic SWNTs for comparison with the hyperbolic band structure of semiconducting SWNTs. When a back gate voltage V_g is applied in **a** relative to the charge neutral point V_{cnp}, the Fermi level E_F indicated by the horizontal dashed blue lines in metallic and semiconducting SWNTs can be continuously tuned.

The electronic band structures of metallic and semiconducting SWNTs are illustrated in Figs. 1b and 1c, respectively[26]. Metallic nanotubes feature a gapless linear band dispersion, $E = \hbar v_0 k_F$, where $\hbar$ is the reduced Planck's constant, $v_0 \sim 0.8 \times 10^6\ m/s$ is the Fermi Velocity in graphene, and k_F is the Fermi wavevector. Their 1D linear bands provide an ideal realization of the linear Luttinger liquid. Semiconducting nanotubes, in contrast, have a finite band gap E_g and feature a hyperbolic dispersion, $E^2 = (E_g/2)^2 + (\hbar v_0 k_F)^2$, where E_g is inversely proportional to the nanotube diameter d as $E_g = 0.75eV/d\ (nm)$. When a back gate voltage V_g is applied (Fig. 1a) relative to the charge neutral point V_{cnp}, the Fermi level E_F in both metallic and semiconducting SWNTs can be continuously tuned from hole doping to charge neutrality and to electron doping as illustrated in Figs. 1b and 1c. The charge neutral point V_{cnp} is the gate voltage needed to offset the unintentional doping usually coming from the substrate.

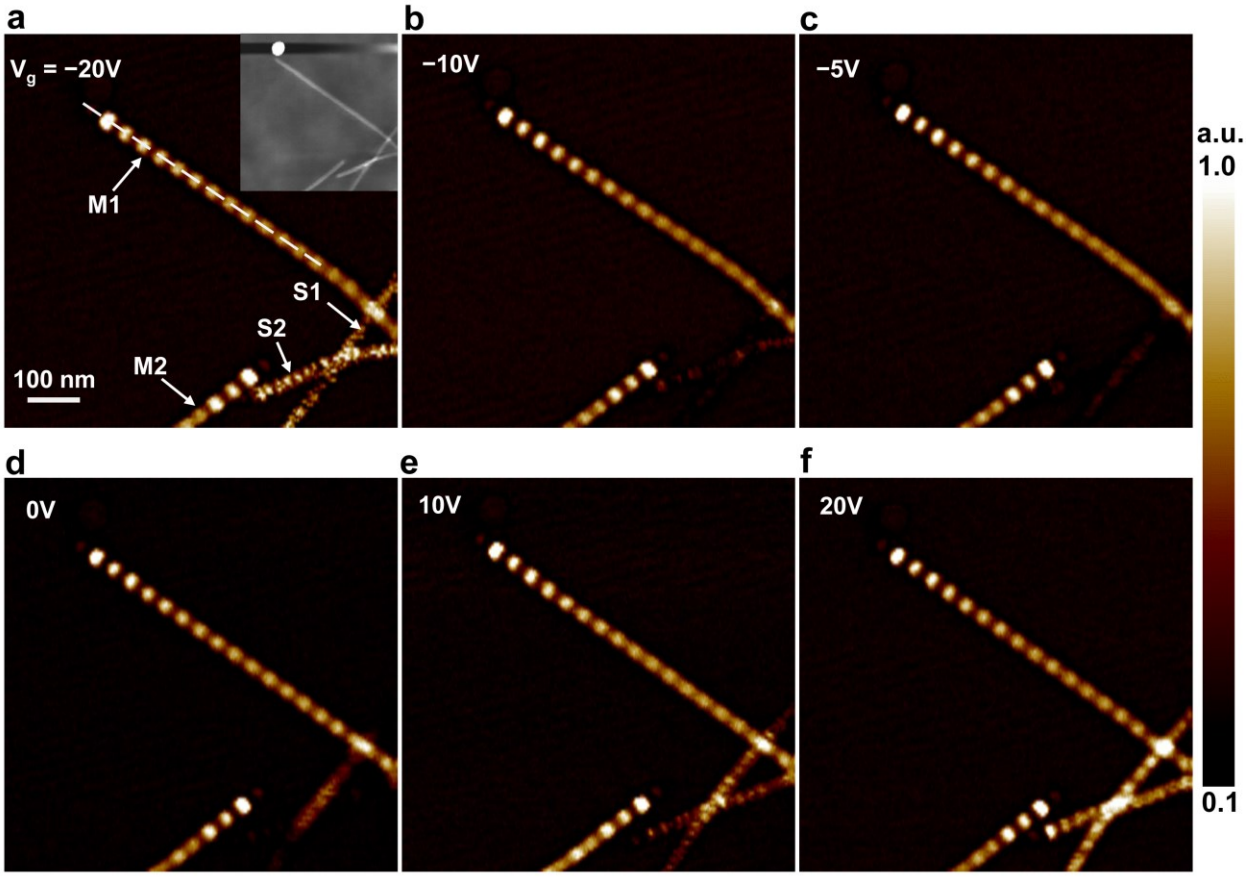

Figure 2| Infrared nano-imaging of metallic and semiconducting SWNTs at different gate voltages. From **a** to **f**, the gate voltage is varied from -20 to 20V. The carrier density changes from hole doping to charge neutrality and then to electron doping. The plasmon features in metallic nanotubes labeled as M1 and M2 in **a** are largely unchanged. In marked comparison, near-field optical responses in semiconducting nanotubes labeled as S1 and S2 in **a** depend sensitively on gate voltages. The line profiles along the nanotube (indicated by the white dashed line in **a**) reveal how the plasmon wave in metallic nanotube M1 gets damped as it propagates. The profiles for different gate voltages (**a** to **f**) are plotted in Fig. S2a. The inset in **a** shows the topography recorded simultaneously with the near-field images.

In Fig. 2, we systematically investigate the dependence of plasmon behaviors on carrier density in semiconducting SWNTs and compare that with plasmon behaviors in doped metallic SWNTs. When gate voltage V_g is varied from -20 to 20 V, the carrier type in SWNTs changes from hole doping to charge neutrality and then to electron doping. The near-field optical responses at these different gate voltages are shown in Figs. 2a to 2f. The topography recorded simultaneously is shown in the top right inset in Fig. 2a. In the near-field images, nanotubes labeled as M1 and M2 in Fig. 2a exhibit prominent oscillation peaks at all gate voltages (Figs. 2a to 2f). These are gapless metallic SWNTs with linear dispersion. The peaks in the near-field images correspond to the constructive interference between the plasmon wave launched by the tip and that

reflected by the nanotube end. Plasmon wavelength can be simply determined as twice the oscillation period. By fitting the line profiles along the nanotubes in the near-field images at different gate voltages with a damped oscillator form $e^{-2\pi x/(Q\cdot\lambda_p)}\sin\left((4\pi x)/\lambda_p\right)$, we can determine the plasmon wavelength λ_p to be ~ 90 nm and the quality factor Q to be ~ 22 and observe that they are largely unchanged at different gate voltages. Plasmon velocity can be determined from $v_p = \lambda_p f \sim 2.5 \times 10^6\, m/s$ where f ~ 28.3 THz is the frequency of the excitation light. The Luttinger liquid parameter g, describing the interaction in SWNTs, can then also be determined to be $g = v_0/v_p \sim 0.31$, which indicates strong coulomb repulsion between electrons in metallic SWNTs. In marked comparison, near-field optical responses in nanotubes labeled as S1 and S2 in Fig. 2a depend sensitively on gate voltages. These two nanotubes correspond to semiconducting SWNTs with hyperbolic dispersion. When the carrier density is near charge neutrality (Fig. 2c), the near-field response is dramatically depleted and we observe weak contrast against the substrate. At substantial doping, well-defined plasmon features emerge and evolve with the gate voltage in both semiconducting nanotubes. The distinctly different plasmon behaviors highlight the critical role of nonlinear band dispersion in semiconducting SWNTs which goes beyond the conventional linear Luttinger liquid paradigm in metallic SWNTs.

Next we examine comprehensively the plasmon behaviors in semiconducting nanotubes and their dependence on carrier density. Fig. 3a shows the topography of a semiconducting nanotube and the inset blue curve shows the height profile along the white dashed line across the nanotube. The diameter is determined to be 2 nm from the height profile and the nanotube thus has a band gap of ~ 0.37 eV. The near-field responses of the nanotube at different gate voltages from -20 to 24 V are presented in Figs. 3b to 3l. The near-field response evolves in a systematic manner, which is consistent with the semiconducting SWNTs in Fig. 2. At $V_g = -5V$ (Fig. 3e), the response is almost completely depleted, which corresponds to the charge neutral point. When carrier density is increased to either hole-doped side (Figs. 3b to 3d) or electron-doped side (Figs. 3f to 3l), there is an increase in the near-field optical response and well-defined plasmons emerge at substantial doping as manifested by the oscillation peaks near the nanotube end. Line profiles along the dashed line in Fig. 3b reveal how the plasmon wave is damped as it propagates (Fig. S2b). By fitting the line profiles with a damped oscillator form, we can extract both the plasmon wavelength and quality factor as a function of gate voltage. The results are summarized in Figs. 4b and 4d. It is evident that plasmons in the semiconducting SWNT can be continuously tuned by means of electrostatic gating. With increasing gate voltage and thus higher Fermi level, the plasmon wavelength increases and the quality factor also shows concomitant growth. Below a critical carrier density indicated by the dashed line in Fig. 4b, the damping is too large to support well-defined plasmons.

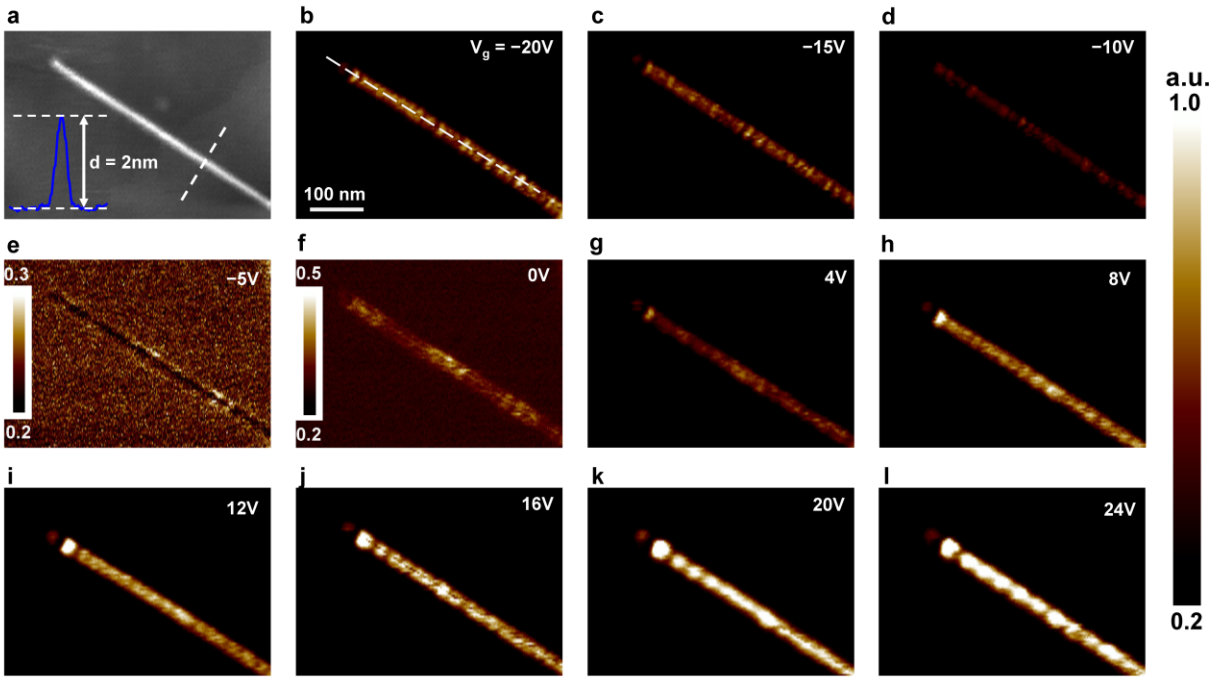

Figure 3| Gate-tunable plasmons in semiconducting SWNTs. a, AFM topography of a semiconducting nanotube. The inset blue curve is the height profile along the white dashed line across the nanotube and the diameter is determined to be 2 nm from the profile. **b** to **l**, Near-field responses of the semiconducting nanotube at different gate voltages from -20 to 24V. Plasmons in the semiconducting SWNT can be continuously tuned by means of electrostatic gating. With increasing gate voltage and thus higher Fermi level, the plasmon wavelength increases and the quality factor also shows concomitant growth. The figures share the same color scale (to give a direct comparison of the infrared responses at different gate voltages) except for **e** and **f,** where the scales shown in insets are intentionally made smaller to offer better contrast between the nanotube and the substrate. The line profiles along the nanotube (indicated by the white dashed line in **b**) reveal how the plasmon wave in the semiconducting nanotube gets damped as it propagates. The profiles for different gate voltages (**h** to **i**) are plotted in Fig. S2b.

As observed in Fig. 2, the gate-independent plasmon behavior in metallic SWNTs is well described by linear Luttinger liquid theory[13, 23, 24]. For an individual suspended carbon nanotube of radius R screened by a concentric metal shell of radius R_s, the linear Luttinger liquid theory predicts the Luttinger liquid interaction parameter g to be

$$\frac{1}{g} = \frac{v_p}{v_F} = \sqrt{1 + \frac{8e^2}{4\pi\varepsilon_{eff}\pi\hbar v_F}\ln(\frac{R_s}{R})}$$

where v_p is the velocity of the collective charge mode, i.e. plasmon velocity, v_F is the Fermi velocity and ε_{eff} is the effective dielectric constant due to substrate screening. This parameter g describes the interaction type and strength in a Luttinger liquid and is only a function of Fermi velocity and the ratio R_s/R for a nanotube under given dielectric environment. The plasmon

wavelength λ_p for a given frequency f is related to g as $\lambda_p = v_p/f = v_F/(gf)$. Because the Fermi velocity is a constant in metallic SWNTs, all the Luttinger liquid phenomena related to g, including the plasmon excitations, will remain the same regardless of carrier density.

In contrast, the gate-tunable plasmon wavelength in semiconducting nanotubes stems from the hyperbolic band dispersion, where the Fermi velocity v_F depends on carrier density. As illustrated in Fig. 4a, the Fermi velocity indicated by the slope of the black tangent line increases with higher Fermi energy. Due to the dominant strong repulsive interaction in SWNTs, plasmon velocity v_p is approximately proportional to $\sqrt{v_F}$ and plasmon wavelength in semiconducting nanotubes with band gap E_g depend on Fermi wavevector k_F as:

$$\lambda_p = \lambda_{p0}\sqrt{\frac{v_F}{v_0}} = \lambda_{p0}\sqrt{\frac{\hbar v_0 k_F}{\sqrt{(E_g/2)^2 + (\hbar v_0 k_F)^2}}}$$

where λ_{p0} and v_0 are the plasmon wavelength and Fermi velocity in metallic nanotubes for a given frequency. Thus one can expect that the plasmon wavelength in semiconducting nanotubes will increase and progressively approach that in metallic ones with larger k_F. The experimentally observed tunable plasmon wavelength at substantially high doping in semiconducting nanotubes (Figs. 3h to 3l) is well reproduced by the theoretical model (Fig. 4b). In this fitting we have used $k_F = \frac{\pi}{4}n = \frac{\pi}{4}\beta C_g|V_g - V_{cnp}|$, where n is the carrier density, C_g is the geometric capacitance, β is a fitting parameter and indicates the overall gate efficiency.

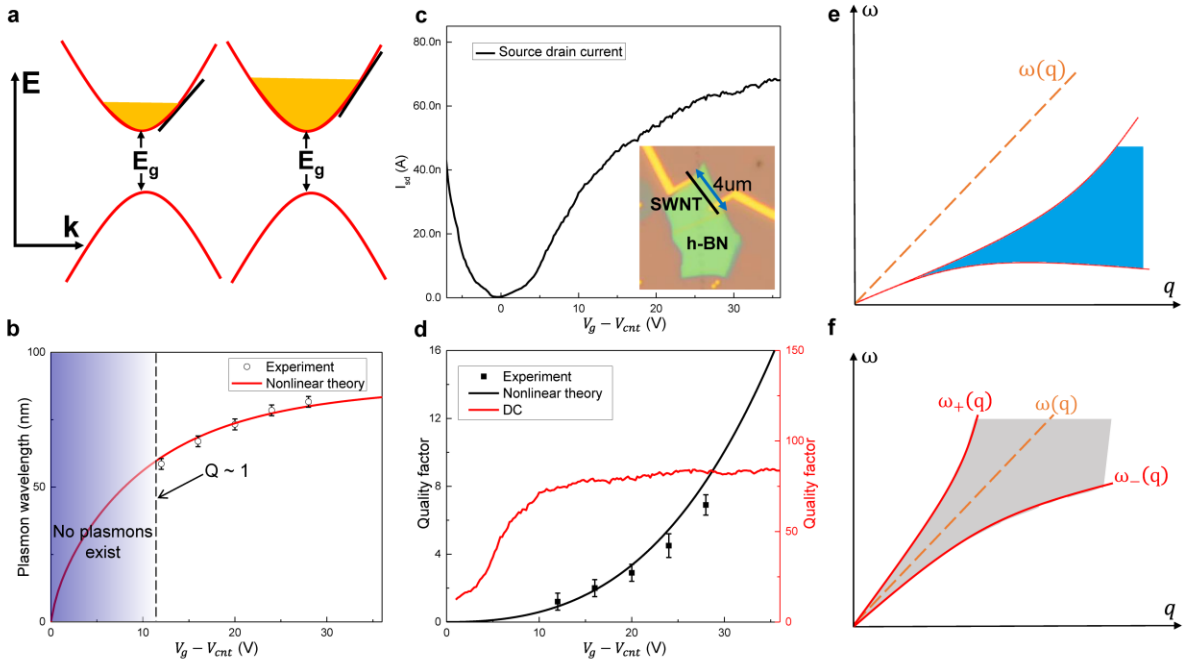

Figure 4| Nonlinear Luttinger liquid model and comparison with experimental results. a, Illustrative hyperbolic energy-momentum (E-k) dispersion (red curve) and Fermi energy (filled yellow region) of a semiconducting SWNT with a band gap E_g. The Fermi velocity indicated by

the slope of the black tangent line increases with higher Fermi energy. **b**, Dependence of plasmon wavelength on gate voltage agrees well with the theoretical model. Below a critical doping indicated by the dashed line (shaded blue area), the plasmon quality factor Q is not large enough for well-defined plasmons to exist. **c**, I_{sd}-V_g (source drain current-gate voltage) curve for a 2 nm diameter semiconducting nanotube at a bias $V_{sd} = 6\,mV$. The inset is an optical image of the device with a channel length of ~ 4 μm. **d**, The nonlinear theory (black line) can well reproduce the experimental dependence of quality factor on gate voltage (black symbols). On the other hand, the plasmon quality factor will be very high and exhibit a completely different gate dependence (red line and right scale) if the damping rate is the same as the electron scattering rate inferred from DC transport measurements. **e**, Illustration of the plasmon dispersion within the RPA. Here the plasmon excitation, ω(q), indicated by the orange dashed line always lies outside the electron-hole continuum indicated by the blue shaded area and is thus free from Landau damping. **f**, Illustrative diagram of DSF from the universal nonlinear Luttinger liquid theory. In a nonlinear Luttinger liquid, the plasmon mode indicated by the gray shaded area is not an exact eigenstate $\omega(\mathrm{q}) = v_p q$ but is broadened with upper and lower bound $\omega_{\pm}(\mathrm{q}) = v_p q \pm q^2/2\tilde{m}$. Error bars in **b** and **d** indicate a 95% confidence interval determined from the curve fitting of the line profiles along the nanotube in Fig. 3 with a damped oscillator form.

Apart from the tunable plasmon wavelength, the quality factor also depends sensitively on gate voltage as shown in Fig. 4d. The tunable damping behaviors are reminiscent of those in graphene plasmons, which can be captured by Landau damping within the random-phase approximation (RPA). The gate-dependent plasmon damping behavior in semiconducting nanotubes shown in Figs. 3h to 3l, however, cannot be explained by this simple picture. No interband damping can exist in a semiconducting nanotube due to its large band gap (~ 0.37 eV) compared to the excitation energy (~ 0.10 eV). It has also been shown that 1D plasmons will not decay to a single electron-hole pair through intraband scattering within the RPA[27]. As illustrated in Fig. 4e, within the RPA theory, the plasmon excitation, $\omega(\mathrm{q})$, indicated by the orange dashed line, always lies outside the electron-hole continuum indicated by the blue shaded area, and thus is free from Landau damping.

We can rule out defect and/or acoustic phonon scattering as a main contribution to the plasmon damping by comparing the infrared near-field nanoscopy results with the electronic transport in semiconducting SWNTs with the same diameter and growth conditions. Fig. 4c displays the gate-dependent DC transport data of a representative SWNT with a diameter of 2 nm and a channel length L of 4 μm by recording the source drain current I_{sd} for different gate voltages at a bias of $V_{sd} = 6\,mV$. The optical image of the SWNT device is shown in the inset. From the measured gate-dependent 1D channel resistance R, we can estimate the mean free path $L_m = \frac{L}{R4e^2/h-1}$ and scattering time $\tau = L_m/v_F$ at different gate voltages. The scattering of electrons close to the Fermi surface, which dominates the electronic transport, is mainly due to defects and acoustic phonons in semiconducting SWNTs at room temperature[28, 29]. We obtain an electron scattering

time longer than 300 fs, corresponding to a scattering rate of ~ $3ps^{-1}$, for carrier density approaching the saturation region for the semiconducting nanotube, which is consistent with previous findings in electronic transport studies of high-quality semiconducting SWNTs[29, 30]. This electron scattering rate is over an order of magnitude smaller than the observed plasmon damping rate. If we assume plasmon damping to have similar origins as the DC transport (i.e. dominated by defect and acoustic phonon scattering), the quality factor determined by $\omega\tau$ will be very high and exhibit a completely different gate dependence (red line and right scale in Fig. 4d) compared with the plasmon behavior. Our experimental data cannot be accounted for by emission of optical phonons either, because the optical phonon scattering should have a weaker dependence on the doping concentration.

The observed unusual gate-dependent plasmon damping in semiconducting nanotubes, on the other hand, can be naturally understood as a consequence of the strong plasmon-plasmon coupling in a nonlinear Luttinger liquid: in metallic nanotubes with prefect linear dispersion, the plasmon excitations are free long-lived bosons without an intrinsic relaxation mechanism within the linear Luttinger liquid theory paradigm. The nonlinear band dispersion in semiconducting nanotubes, however, can enable extremely strong coupling between different plasmon modes because they all propagate at the same speed. As a result, a high-energy plasmon can efficiently decay into multiple low-energy plasmons in semiconducting nanotubes.

A universal description of the dynamic response function in a nonlinear Luttinger liquid has been theorized previously[17, 21]. The dynamic excitation of plasmons in a 1D system is determined by the dynamic structure factor (DSF). For a linear Luttinger liquid as in metallic SWNTs, the DSF takes the form $\mathrm{S}(\mathrm{q},\omega) = 2g|q|\delta(\omega - v_p q)$. This suggests that the plasmon mode features a linear dispersion $\omega(\mathrm{q}) = v_p q$ indicated by the dashed orange line in Fig. 4f and is free of intrinsic relaxation. For a nonlinear Luttinger liquid as in gated semiconducting SWNTs, the DSF is given by

$$\mathrm{S}(\mathrm{q},\omega) = 2\frac{\widetilde{m}g}{|q|}\theta\left(\frac{q^2}{2\widetilde{m}} - \left|\omega - v_p q\right|\right)$$

with an effective mass $\widetilde{m}$. The effective mass $\widetilde{m}$ depends on electron-electron interactions and it can be expressed as $\frac{1}{\widetilde{m}} = \frac{v_p}{2g}\frac{\partial}{\partial E_F}(v_p\sqrt{g})$. The plasmon mode is thus not an exact eigenstate but is broadened with upper and lower bound $\omega_{\pm}(\mathrm{q}) = v_p q \pm q^2/2\widetilde{m}$, as indicated by the red lines in Fig. 4f. The width of the broadening is $\delta\omega(q) = q^2/\widetilde{m}$. For a given frequency, a set of plamson modes with different momenta can be excited in the shaded gray area where DSF differs from zero. This broadening reflects the finite lifetime and damping of the plasmons. As the Fermi energy E_F increases compared to the excitation energy ω, the broadening becomes less severe and well-defined plasmons begin to emerge in agreement with experimental observations.

This dissipation reflected in the broadening of the DSF can be further quantitatively characterized as $\delta\omega/\omega = \omega/\widetilde{m}v_p^2$. In semiconducting nanotubes with hyperbolic dispersion, this

broadening depends on Fermi wavevector k_F as

$$\frac{\delta\omega}{\omega} = \frac{3\sqrt{3}}{8}\left(\frac{\sqrt{\left(E_g/2\right)^2 + (\hbar v_0 k_F)^2}}{\hbar v_0 k_F}\right)^{\frac{5}{4}} \frac{(E_g/2)^2}{(E_g/2)^2 + (\hbar v_0 k_F)^2}\frac{\omega}{v_0 k_F}$$

The plasmon quality factor determined by this nonlinear dispersion can be described as $\omega/\delta\omega$ and its dependence on gate voltage is depicted in Fig. 4d. The nonlinear theory (black line) can well reproduce the experimental results (black symbols). With increasing carrier density and Fermi energy, the band structure gradually approaches linear dispersion. This decrease in the nonlinearity of dispersion leads to the increase of plasmon lifetime and a higher quality factor observed in the experiments. The small discrepancy might indicate that other damping mechanisms also play a role, but nevertheless, are not dominant in our experiment. We conclude that in doped semiconducting nanotubes with hyperbolic dispersion, at the high-energy regime where excitation energy is comparable to Fermi energy, the system should be described as a nonlinear Luttinger liquid and the plasmon damping mechanism is dominated intrinsically by the nonzero curvature of the band dispersion. Note that if we probe at the low-energy regime where excitation energy is much smaller than Fermi energy, $\delta\omega/\omega$ will be vanishingly small and the system will reproduce the linear Luttinger liquid regime. The intriguing gate dependent nonlinear Luttinger liquid plasmon behaviors offer the alluring capability of active electrical switching and tuning of plasmons in semiconducting nanotubes. The highly confined and tunable plasmons and their compatibility with FET devices hold great promise for novel nanophotonic applications[31, 32].

Methods

Carbon nanotube growth and device fabrications. Ferritin solution (0.1 mmol/L) is drop-casted onto SiO_2 (285 nm)/Si substrates. The substrates are then rinsed with isopropyl alcohol (IPA) and are subsequently blew drying. The substrates are annealed in air at 900 ℃ for 30 minutes to convert ferritin to Fe_2O_3, which acts as catalysts for SWNTs growth. Hexagonal boron nitride (h-BN) flakes are then mechanically exfoliated onto the SiO_2/Si substrates with Fe_2O_3. High-quality SWNTs are then directly grown on the substrates by chemical vapor deposition (CVD). We use an ambient-pressure CVD system equipped with a one-inch quartz tube. The system is firstly purged with hydrogen gas for 10 minutes to get rid of the air. After that, the temperature is raised to 900 °C in 15 minutes under 300 sccm of hydrogen flow. When the temperature reaches 900 °C, 110 sccm of argon is introduced through a bubbler with ethanol, which works as the carbon precursor, while 300 sccm of hydrogen flow is maintained to reduce iron compound nanoparticles to iron nanoparticles. The temperature is kept at 900 °C for 15 minutes, followed by naturally cooling down to room temperature under a hydrogen flow of 300 sccm. Electrical contacts on SWNTs are then fabricated using standard e-beam lithography or shadow masks. For individual nanotube transport measurement, SWNTs on SiO_2 are thoroughly eliminated by oxygen plasma with the nanotube between the electrodes left for transport measurement. Shadow masks are used to define one contact for back gating to avoid polymer contamination and to keep the nanotubes ultraclean

for gate controlled infrared nano-imaging. E-beam lithography is used to define electrodes for electronic transport measurements.

Infrared nano-imaging of carbon nanotube plasmons. The scattering-type SNOM for this work is based on a tapping mode AFM (Bruker Innova). For infrared nano-imaging, a CO_2 laser with wavelength 10.6 μm is focused onto the apex of a gold-coated AFM tip (Nanoandmore) with a radius of tip apex ~ 20 nm. The tapping frequency and amplitude of the tip are $\Omega \sim 240$ kHz and ~ 80 nm, respectively. The backscattered signal from the tip apex carries local optical information of the sample and is captured by a Mercury cadmium telluride (MCT) detector in the far field. The detector signal is demodulated at a frequency 3Ω by a lock-in amplifier (Zurich Instruments HF2LI) to suppress the background scattering from the tip shaft and sample. By a raster scanning of the sample, near-field images are obtained simultaneously with the topography.

References:

[1] S.-i. Tomonaga, Remarks on Bloch's method of sound waves applied to many-fermion problems, Progress of Theoretical Physics, 5 (1950) 544-569.

[2] J.M. Luttinger, An Exactly Soluble Model of a Many-Fermion System, Journal of Mathematical Physics, 4 (1963) 1154-&.

[3] F.D.M. Haldane, 'Luttinger liquid theory' of one-dimensional quantum fluids. I. Properties of the Luttinger model and their extension to the general 1D interacting spinless Fermi gas, Journal of Physics C: Solid State Physics, 14 (1981) 2585.

[4] T. Giamarchi, Quantum physics in one dimension, Oxford university press2004.

[5] Electrons in one dimension and the Luttinger liquid, in: G. Giuliani, G. Vignale (Eds.) Quantum Theory of the Electron Liquid, Cambridge University Press, Cambridge, 2005, pp. 501-549.

[6] V.V. Deshpande, M. Bockrath, L.I. Glazman, A. Yacoby, Electron liquids and solids in one dimension, Nature, 464 (2010) 209-216.

[7] J. Voit, One-Dimensional Fermi Liquids, Reports on Progress in Physics, 58 (1995) 977-1116.

[8] M. Bockrath, D.H. Cobden, J. Lu, A.G. Rinzler, R.E. Smalley, L. Balents, P.L. McEuen, Luttinger-liquid behaviour in carbon nanotubes, Nature, 397 (1999) 598-601.

[9] Z. Yao, H.W.C. Postma, L. Balents, C. Dekker, Carbon nanotube intramolecular junctions, Nature, 402 (1999) 273-276.

[10] H. Ishii, H. Kataura, H. Shiozawa, H. Yoshioka, H. Otsubo, Y. Takayama, T. Miyahara, S. Suzuki, Y. Achiba, M. Nakatake, T. Narimura, M. Higashiguchi, K. Shimada, H. Namatame, M. Taniguchi, Direct observation of Tomonaga-Luttinger-liquid state in carbon nanotubes at low temperatures, Nature, 426 (2003) 540-544.

[11] Y. Jompol, C.J.B. Ford, J.P. Griffiths, I. Farrer, G.A.C. Jones, D. Anderson, D.A. Ritchie, T.W. Silk, A.J. Schofield, Probing Spin-Charge Separation in a Tomonaga-Luttinger Liquid, Science, 325 (2009) 597-601.

[12] S. Zhao, S. Wang, F. Wu, W. Shi, I.B. Utama, T. Lyu, L. Jiang, Y. Su, S. Wang, K. Watanabe, T. Taniguchi, A. Zettl, X. Zhang, C. Zhou, F. Wang, Correlation of Electron Tunneling and Plasmon Propagation in a Luttinger Liquid, Physical Review Letters, 121 (2018) 047702.

[13] C. Kane, L. Balents, M.P.A. Fisher, Coulomb interactions and mesoscopic effects in carbon nanotubes, Physical Review Letters, 79 (1997) 5086-5089.

[14] R. Egger, A.O. Gogolin, Effective Low-Energy Theory for Correlated Carbon Nanotubes, Physical Review Letters, 79 (1997) 5082-5085.
[15] P.F. Williams, A.N. Bloch, Self-consisten dielectric response of a quasi-one-dimensional metal at high frequencies, Physical Review B, 10 (1974) 1097-1108.
[16] M. Pustilnik, M. Khodas, A. Kamenev, L.I. Glazman, Dynamic Response of One-Dimensional Interacting Fermions, Physical Review Letters, 96 (2006) 196405.
[17] A. Imambekov, L.I. Glazman, Universal Theory of Nonlinear Luttinger Liquids, Science, 323 (2009) 228-231.
[18] A. Imambekov, L.I. Glazman, Phenomenology of One-Dimensional Quantum Liquids Beyond the Low-Energy Limit, Physical Review Letters, 102 (2009) 126405.
[19] G. Barak, H. Steinberg, L.N. Pfeiffer, K.W. West, L. Glazman, F. von Oppen, A. Yacoby, Interacting electrons in one dimension beyond the Luttinger-liquid limit, Nature Physics, 6 (2010) 489.
[20] T.L. Schmidt, A. Imambekov, L.I. Glazman, Spin-charge separation in one-dimensional fermion systems beyond Luttinger liquid theory, Physical Review B, 82 (2010) 245104.
[21] A. Imambekov, T.L. Schmidt, L.I. Glazman, One-dimensional quantum liquids: Beyond the Luttinger liquid paradigm, Reviews of Modern Physics, 84 (2012) 1253-1306.
[22] Y. Jin, O. Tsyplyatyev, M. Moreno, A. Anthore, W.K. Tan, J.P. Griffiths, I. Farrer, D.A. Ritchie, L.I. Glazman, A.J. Schofield, C.J.B. Ford, Momentum-dependent power law measured in an interacting quantum wire beyond the Luttinger limit, Nature Communications, 10 (2019) 2821.
[23] S. Wang, F. Wu, S. Zhao, K. Watanabe, T. Taniguchi, C. Zhou, F. Wang, Logarithm Diameter Scaling and Carrier Density Independence of One-Dimensional Luttinger Liquid Plasmon, Nano Letters, 19 (2019) 2360-2365.
[24] Z. Shi, X. Hong, H.A. Bechtel, B. Zeng, M.C. Martin, K. Watanabe, T. Taniguchi, Y.-R. Shen, F. Wang, Observation of a Luttinger-liquid plasmon in metallic single-walled carbon nanotubes, Nat Photon, 9 (2015) 515-519.
[25] M. Liu, A.J. Sternbach, D.N. Basov, Nanoscale electrodynamics of strongly correlated quantum materials, Reports on Progress in Physics, 80 (2016) 014501.
[26] R. Saito, G. Dresselhaus, M.S. Dresselhaus, Physical Properties of Carbon Nanotube, Imperial College Press1998.
[27] S. Das Sarma, E.H. Hwang, Dynamical response of a one-dimensional quantum-wire electron system, Physical Review B, 54 (1996) 1936-1946.
[28] M.J. Biercuk, S. Ilani, C.M. Marcus, P.L. McEuen, Electrical Transport in Single-Wall Carbon Nanotubes, in: A. Jorio, G. Dresselhaus, M.S. Dresselhaus (Eds.) Carbon Nanotubes: Advanced Topics in the Synthesis, Structure, Properties and Applications, Springer Berlin Heidelberg, Berlin, Heidelberg, 2008, pp. 455-493.
[29] X. Zhou, J.-Y. Park, S. Huang, J. Liu, P.L. McEuen, Band Structure, Phonon Scattering, and the Performance Limit of Single-Walled Carbon Nanotube Transistors, Physical Review Letters, 95 (2005) 146805.
[30] M.S. Purewal, B.H. Hong, A. Ravi, B. Chandra, J. Hone, P. Kim, Scaling of Resistance and Electron Mean Free Path of Single-Walled Carbon Nanotubes, Physical Review Letters, 98 (2007) 186808.
[31] X. He, H. Htoon, S.K. Doorn, W.H.P. Pernice, F. Pyatkov, R. Krupke, A. Jeantet, Y. Chassagneux, C. Voisin, Carbon nanotubes as emerging quantum-light sources, Nature Materials, DOI 10.1038/s41563-018-0109-2(2018).
[32] E. Ozbay, Plasmonics: Merging Photonics and Electronics at Nanoscale Dimensions, Science, 311 (2006) 189-193.

Data availability: The data that support the findings of this study are available from the corresponding author upon reasonable request.

Code availability: Matlab codes for nonlinear theory calculation are available from the

corresponding author upon reasonable request.

Acknowledgments: The authors thank Prof. Norman Yao, Dr. Romain Vasseur, Dr. Jihun Kang and Halleh B. Balch for helpful discussions. This work was mainly supported by the Director, Office of Science, Office of Basic Energy Sciences, Materials Sciences and Engineering Division of the U.S. Department of Energy under Contract No. DE-AC02-05-CH11231 (sp2-Bonded Materials Program KC2207). The device fabrication and electrical measurement were supported by the Office of Naval research (MURI award N00014-16-1-2921). The data analysis was supported by the NSF award 1808635. Z.S. acknowledge support from National Natural Science Foundation of China (11774224 and 11574204). Fanqi W., Z. Z. and C.Z. acknowledge National Science Foundation for financial support under Grant No. 769K521. K.W. and T.T. acknowledge support from the Elemental Strategy Initiative conducted by the MEXT, Japan and the CREST (JPMJCR15F3), JST.

Author contributions: F.W., S.W., Z.S. conceived the project and designed the experiment. F.W. and C.Z supervised the project. S.W. fabricated the devices and performed the infrared nano-imaging measurements. S.Z. and S.W. fabricated the devices for the transport measurements and carried out the electrical measurements. Fanqi W. and Z.Z. under the supervision of C.Z. grew the SWNTs samples and performed SEM. Z.S., L.J., A.Z. assisted in device fabrications. K.W. and T.T. provided the h-BN crystals. S.W. and F.W. analyzed the data. All authors contributed to the writing of the manuscript.

Competing interests: The authors declare no competing interests.

Additional information:

Supplementary information is available for this paper.

Correspondence and requests for materials should be addressed to F.W..

Reprints and permissions information is available at www.nature.com/reprints.